Citation: CPT Pharmacometrics Syst. Pharmacol. (2018) 00, 00; doi:10.1002/psp4.12275

ORIGINAL ARTICLE

Comprehensive PBPK Model of Rifampicin for Quantitative Prediction of Complex Drug-Drug Interactions: CYP3A/2C9 Induction and OATP Inhibition Effects

Ryuta Asaumi[1], Kota Toshimoto[2], Yoshifusa Tobe[1], Kenta Hashizume[3], Ken-ichi Nunoya[1], Haruo Imawaka[1], Wooin Lee[4] and Yuichi Sugiyama[2]*

This study aimed to construct a physiologically based pharmacokinetic (PBPK) model of rifampicin that can accurately and quantitatively predict complex drug-drug interactions (DDIs) involving its saturable hepatic uptake and auto-induction. Using *in silico* and *in vitro* parameters, and reported clinical pharmacokinetic data, rifampicin PBPK model was built and relevant parameters for saturable hepatic uptake and UDP-glucuronosyltransferase (UGT) auto-induction were optimized by fitting. The parameters for cytochrome P450 (CYP) 3A and CYP2C9 induction by rifampicin were similarly optimized using clinical DDI data with midazolam and tolbutamide as probe substrates, respectively. For validation, our current PBPK model was applied to simulate complex DDIs with glibenclamide (a substrate of CYP3A/2C9 and hepatic organic anion transporting polypeptides (OATPs)). Simulated results were in quite good accordance with the observed data. Altogether, our constructed PBPK model of rifampicin demonstrates the robustness and utility in quantitatively predicting CYP3A/2C9 induction-mediated and/or OATP inhibition-mediated DDIs with victim drugs.
CPT Pharmacometrics Syst. Pharmacol. (2018) **00**, 00; doi:10.1002/psp4.12275; published online on 0 Month 2018.

Study Highlights

WHAT IS THE CURRENT KNOWLEDGE ON THE TOPIC?

☑ Rifampicin, an inducer of CYP3A/2C9 and an inhibitor of OATPs, is associated with many DDIs. A well-constructed PBPK model will allow for quantitative prediction of DDIs.

WHAT QUESTION DID THIS STUDY ADDRESS?

☑ This study constructed a PBPK model of rifampicin incorporating its saturable hepatic uptake and auto-induction to predict CYP3A/2C9 induction-mediated and OATP inhibition-mediated DDIs. Relevant parameters of rifampicin were obtained via stepwise optimization using the nonlinear and auto-induction pharmacokinetic data and DDI data with midazolam and tolbutamide as probe substrates. The obtained parameters were applied to simulate complex DDIs with glibenclamide (a substrate for both CYP3A/2C9 and OATPs).

WHAT DOES THIS STUDY ADD TO OUR KNOWLEDGE?

☑ The constructed PBPK model adequately captured *in vivo* CYP3A/2C9 induction effects in the liver and small intestine, and successfully predicted the CYP3A/2C9 induction-mediated and/or OATP inhibition-mediated DDIs with glibenclamide.

HOW MIGHT THIS CHANGE DRUG DISCOVERY, DEVELOPMENT, AND/OR THERAPEUTICS?

☑ This rifampicin PBPK model presents advancement toward accurate prediction of DDIs with potential victim drugs that are in clinical use or under development.

Rifampicin has been an essential part of tuberculosis therapy for decades. The pharmacokinetics of rifampicin has long been of interest due to its nonlinear and auto-induction behaviors.[1,2] In addition, rifampicin acts as a perpetrator drug for many co-administered drugs, causing clinically relevant drug-drug interactions (DDIs) via induction of metabolic enzymes (e.g., cytochrome P450 (CYP), UDP-glucuronosyltransferases (UGTs)), and/or via inhibition of hepatic organic anion transporting polypeptides (OATPs).[3,4] For instance, rifampicin induces CYP3A and CYP2C9, both of which are main CYP isoforms handling oxidative metabolism for the majority of drug molecules.[3,5] With co-administration of repeated rifampicin doses, drugs that are metabolized by CYP3A and/or CYP2C9 displayed decreases in their systemic exposure and efficacy.[3] On the other hand, statins (substrates of OATPs), upon co-administration with rifampicin, were shown to have an increased systemic exposure (mostly via OATP inhibition),[6,7] thereby increasing the risk for serious adverse events, such as rhabdomyolysis. Cases of complex DDIs have also been reported between rifampicin and co-administered drugs, which are substrates for both metabolic enzymes and OATPs.[8,9] Given that the magnitude of DDIs may well depend on the route, duration, and timing of rifampicin administration, there has been an increasing need for

[1]Pharmacokinetic Research Laboratories, Ono Pharmaceutical Co., Ltd., Tsukuba, Ibaraki, Japan; [2]Sugiyama Laboratory, RIKEN Innovation Center, RIKEN, Yokohama, Kanagawa, Japan; [3]Drug Development Solutions Division, Sekisui Medical Co., Ltd., Ibaraki, Japan; [4]College of Pharmacy and Research Institute of Pharmaceutical Sciences, Seoul National University, Seoul, Korea. *Correspondence: Yuichi Sugiyama (ychi.sugiyama@riken.jp)
Received 2 October 2017; accepted 28 December 2017; published online on 0 Month 2018. doi:10.1002/psp4.12275

correctly and quantitatively predicting DDIs incurred by rifampicin administered in various dosing regimens.

Because DDI prediction using static models utilizes theoretical maximum concentrations of a perpetrator drug at the sites of DDI evaluation, the risk for DDIs tends to be overestimated. Thus, the use of physiologically based pharmacokinetic (PBPK) models has been recommended as a more quantitative approach.[10,11] By considering the concentration-time profiles of both a perpetrator and a victim drug at the sites of DDI evaluation, the PBPK models may offer mechanism-based DDI predictions under various circumstances.

Construction of a PBPK model for DDI predictions involving rifampicin requires two sets of parameters; one for predicting concentration-time profiles of rifampicin in blood and tissues, and the other for predicting DDIs on pharmacokinetics of victim drugs. To properly set these parameters, the following key information was gleaned from the literature.

Rifampicin displays a high bioavailability of ~90% after a single oral dose and it is primarily eliminated in the liver,[12] likely involving OATP-mediated uptake and UGT-mediated metabolism. Rifampicin is a substrate of OATP1B1 (with the reported Michaelis-Menten constant (K_m) value of 1.2 μg/mL) and OATP1B3.[13] After single oral doses of 450 and 600 mg rifampicin, its maximum plasma concentrations (C_{max}) were reported to be 7.3 and 14.4 μg/mL, respectively (the corresponding unbound C_{max} of 0.51 and 1.0 μg/mL, considering its unbound fraction in plasma of 0.07).[14,15] Given that these unbound C_{max} values are quite close to the K_m value for OATP1B1, the saturation of hepatic uptake may well contribute to nonlinear rifampicin pharmacokinetics. After single oral dosing, rifampicin was excreted mainly as water-soluble metabolites (probably, rifampicin glucuronides) in feces or urine.[16] The fractional metabolism (f_m) value of rifampicin for UGT was calculated to be 0.759 from the literature,[16] suggesting that the UGT-mediated metabolism is involved in its auto-induction. Based on these data, we reasoned that the following parameters need to be incorporated into our PBPK model of rifampicin: (i) parameters related to the saturable hepatic uptake and UGT auto-induction; (ii) parameters to estimate unbound rifampicin concentration-time profiles at the DDI sites (e.g., unbound fraction in hepatocytes and enterocytes); (iii) parameters related to the induction of metabolic enzymes (the maximum induction effect (E_{max}) and the concentration for the half maximum induction effect (EC_{50})) and the inhibition of OATPs (the inhibition constant (K_i)).

For construction of PBPK models for victim drugs, it is important to adequately capture their elimination mechanisms. For a victim drug whose elimination involves both hepatic uptake and metabolism, it is necessary to estimate the fractional influx of an affected active uptake pathway as well as the fractional metabolism of an affected metabolic pathway. For example, the antidiabetic agent glibenclamide is primarily eliminated from the liver via OATP-mediated uptake and subsequent metabolism by CYP3A and CYP2C9. Zheng *et al*.[8] reported the case of complex DDIs between glibenclamide and rifampicin, depending on the duration and timing of rifampicin co-administration (involving OATP inhibition and/or CYP3A/2C9 induction by rifampicin). For the construction of a PBPK model of glibenclamide, the accurate estimation for the contribution of hepatic active uptake and passive diffusion, and CYP3A and CYP2C9 metabolism will be necessary.

In setting various parameters of perpetrator and victim drugs, Yoshikado *et al*.[15] proposed a global *in vitro-in vivo* extrapolation method that combines the use of *in vitro* parameters and optimization of *in vivo* parameters, and successfully implemented the proposed method for the analyses of transporter-mediated DDIs. In the present study, we aimed to construct a comprehensive PBPK model of rifampicin that can predict DDIs mediated by CYP3A/2C9 induction and/or OATP inhibition using the global *in vitro-in vivo* extrapolation method. Specifically, the rifampicin PBPK model was constructed based on the *in silico*, *in vitro*, and *in vivo* data. Relevant parameters of rifampicin related to the saturable hepatic uptake and UGT auto-induction were optimized. Thereafter, parameters for CYP3A and CYP2C9 induction by rifampicin were obtained by fitting to clinical DDI data with a probe substrate for CYP3A (midazolam) and CYP2C9 (tolbutamide), respectively. Incorporating these induction parameters as well as our previously reported OATP inhibition parameter of rifampicin,[15] complex DDIs between rifampicin and glibenclamide were finally simulated and compared with the observed data to validate the constructed PBPK model of rifampicin.

METHODS

Construction of PBPK models

The PBPK models were constructed and optimized using the methods described in the previous report[15] and Numeric Analysis Program for Pharmacokinetics, Napp (version 2.31).[17] The nonlinear least-squares fitting was used in the optimization processes with the weight for the calculation set as none or the square root of the value. All nomenclature and differential equations are shown in **Supplementary Text**.

The PBPK models of rifampicin, midazolam, tolbutamide, and glibenclamide were constructed based on their *in silico*, *in vitro*, and clinical pharmacokinetic data available from the literature (**Figure 1**). Each model included the central (blood) compartment, three large-volume tissues (muscle, skin, and adipose), and the liver, which was divided into five compartments tandemly connected by hepatic blood flow (5-liver model) to mimic the dispersion model. For rifampicin and glibenclamide, each liver compartment was further subdivided into extrahepatic and hepatocellular compartments to incorporate the hepatic uptake process of the drugs. For rifampicin, absorption was described by a segregated flow model to accurately capture its unbound concentration-time profile in enterocytes related to its metabolic enzyme induction.[18] For midazolam and glibenclamide, absorption was described by Q_{gut} model to take their intestinal metabolism into consideration.[19] Enterohepatic circulation was not incorporated in any of the constructed models, given that its contribution was negligible for rifampicin and not indicated for the other drugs.[20]

Determination of PBPK model parameters

Basic physiological and pharmacokinetic parameters were obtained either from the previous reports or by calculations

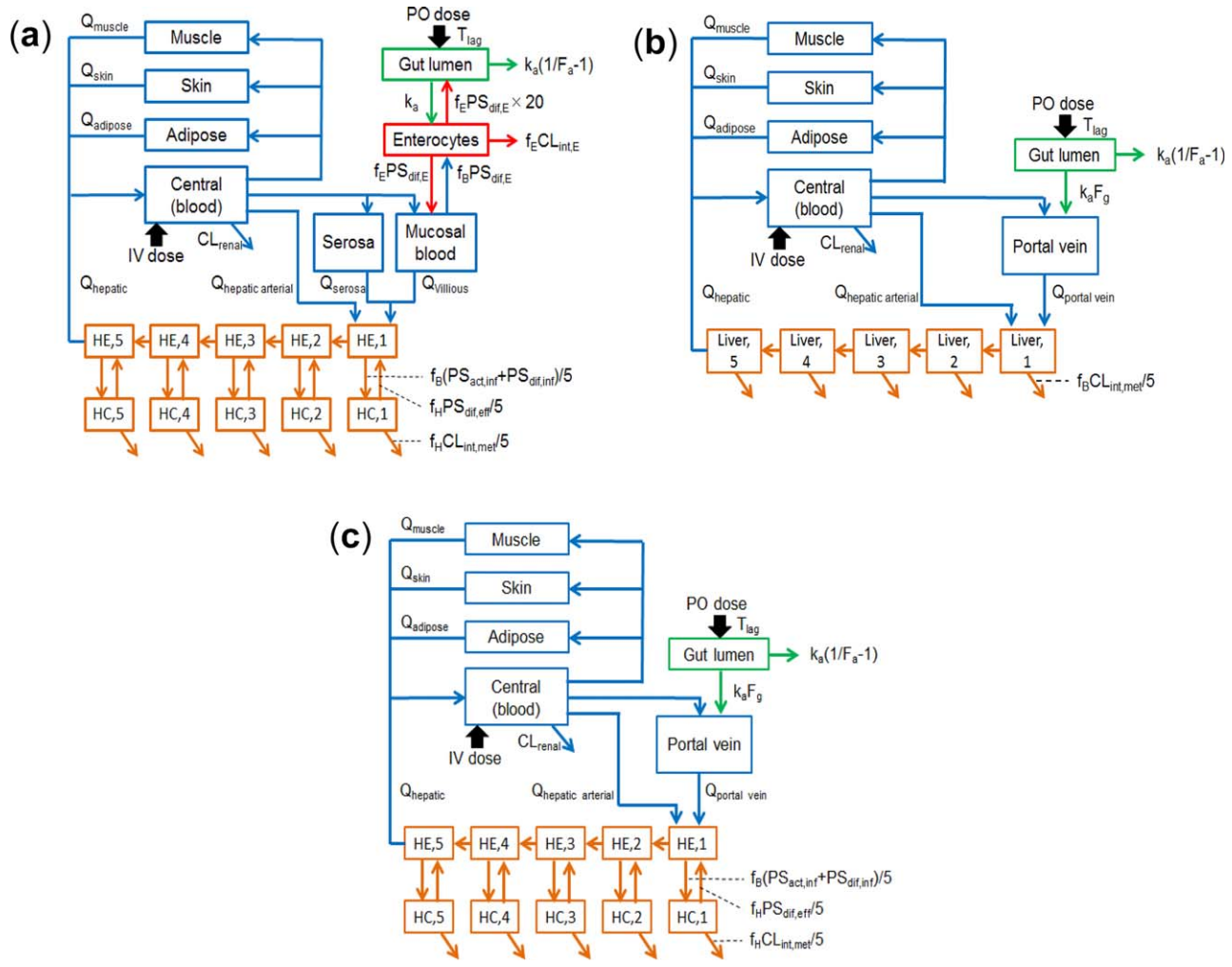

Figure 1 Structures of physiologically based pharmacokinetic (PBPK) models of rifampicin (**a**), midazolam (**b**), tolbutamide (**b**), and glibenclamide (**c**). $CL_{int,E}$, intrinsic clearance of enterocyte metabolism; $CL_{int,met}$, intrinsic clearance of hepatic metabolism; CL_{renal}, renal clearance; F_a, fraction of dose absorbed from the gut lumen; f_B, unbound fraction in blood; f_E, unbound fraction in enterocytes; F_g, fraction available after intestinal metabolism; f_H, unbound fraction in hepatocytes; HC, hepatocytes; HE, hepatic extracellular space; k_a, absorption rate constant; $PS_{act,inf}$, active uptake intrinsic clearance on sinusoidal membrane; $PS_{dif,inf}$, influx intrinsic clearance by passive diffusion through sinusoidal membrane; $PS_{dif,E}$, intrinsic clearance by passive diffusion through basolateral membrane of enterocytes; $PS_{dif,eff}$, efflux intrinsic clearance by passive diffusion through sinusoidal membrane; Q_{tissue}, blood flow rate in tissue; T_{lag}, lag time in intestinal absorption. The rate constant for drug excretion from gut lumen to feces is represented as $k_a(1/F_a\text{-}1)$.

(see **Supplementary Text**, **Supplementary Tables S1 and S2**). The β value is a hybrid parameter reflective of the major rate-limiting steps of overall hepatic intrinsic clearance ($CL_{int,all}$), as described in Eqs. 1 and 2 (the contribution of $CL_{int,bile}$ was deemed minimal for rifampicin and glibenclamide[20]). Due to the difficulties in estimating the parameter β from *in vitro* experiments, sensitivity analyses were performed using three β values (0.2, 0.5, and 0.8) for the models of rifampicin and glibenclamide.

$$CL_{int,all} = \left(PS_{act,inf} + PS_{dif,inf}\right) \times \frac{CL_{int,met}}{PS_{dif,eff} + CL_{int,met}} \quad (1)$$

$$\beta = \frac{CL_{int,met}}{PS_{dif,eff} + CL_{int,met}} \quad (2)$$

When $CL_{int,met}$ is much greater than $PS_{dif,eff}$ (high β), $CL_{int,all}$ can be approximated as PS_{inf} (equal to the sum of $PS_{act,inf}$ and $PS_{dif,inf}$), and the rate-limiting step for $CL_{int,all}$ becomes the hepatic uptake. In contrast, when $CL_{int,met}$ is negligible compared to $PS_{dif,eff}$ (low β), $CL_{int,all}$ can be approximated as $PS_{inf} \times CL_{int,met}/PS_{dif,eff}$ and $CL_{int,all}$ is determined not only by hepatic uptake but also by metabolism. To reflect these different conditions, three β values were selected in this study. For all analyses, dosing regimens were kept similar to the original study designs reported.

The stepwise optimization of the necessary parameters was carried out. Specifically, rifampicin parameters were determined as follows. The distribution volume of rifampicin was adjusted by applying a common scaling factor to *in silico* K_p values of each tissue (SF_{Kp}) by simultaneous fitting to the reported blood rifampicin concentration-time profiles after single intravenous doses of 300 and 600 mg rifampicin.[21] The unbound K_m ($K_{m,u}$) value of rifampicin for hepatic uptake

Table 1 Optimized parameters of rifampicin, midazolam, tolbutamide, and glibenclamide

Parameters		Rifampicin $\beta = 0.2$	Midazolam[a]	Tolbutamide	Glibenclamide $\beta = 0.2$	Glibenclamide $\beta = 0.5$	Glibenclamide $\beta = 0.8$
k_a (/h)		37.6 ± 17.6	1.29 ± 0.21	-	0.445 ± 0.053	0.445 ± 0.053	0.445 ± 0.053
T_{lag} (h)		0.255 ± 0.000	0.031 ± 0.008	-	0.773 ± 0.079	0.773 ± 0.079	0.773 ± 0.079
SF_{Kp}[b]		6.65 ± 0.98	0.201 ± 0.035	0.500 ± 0.073	0.568 ± 0.045	0.571 ± 0.045	0.572 ± 0.045
$f_BCL_{int,all}$ or f_BCL_{int} (L/h/kg)		0.251 ± 0.028	0.469 ± 0.030	0.0151 ± 0.0006	0.123 ± 0.004	0.123 ± 0.004	0.123 ± 0.004
$PS_{dif,E}$ (L/h/kg)		0.161 ± 0.079	-	-	-	-	-
$V_{central}$ (L/kg)		-	0.571 ± 0.050	-	-	-	-
$K_{m,u}$ for hepatic uptake[c]	(ng/mL)	146 ± 45	-	-	-	-	-
	(μmol/L)	0.177 ± 0.055	-	-	-	-	-
$EC_{50,u}$ for enzyme induction	(ng/mL)	52.6 ± 7.5	-	-	-	-	-
	(μmol/L)	0.0639 ± 0.0091	-	-	-	-	-
E_{max} for UGT auto-induction		1.34 ± 0.50	-	-	-	-	-
E_{max} for CYP3A induction		4.57 ± 0.18	-	-	-	-	-
E_{max} for CYP2C9 induction		2.41 ± 0.06	-	-	-	-	-

$\beta = CL_{int,all}/(PS_{act,inf} + PS_{dif,inf})$; CL_{int}, hepatic intrinsic clearance; $CL_{int,all}$, overall hepatic intrinsic clearance; $EC_{50,u}$, unbound concentration for half maximum induction effect; E_{max}, maximum induction effect; f_B, unbound fraction in blood; k_a, absorption rate constant; $K_{m,u}$, unbound Michaelis-Menten constant; K_p, tissue/blood concentration ratio; $PS_{act,inf}$, active uptake intrinsic clearance on sinusoidal membrane; $PS_{dif,inf}$, influx intrinsic clearance by passive diffusion through sinusoidal membrane; $PS_{dif,E}$, intrinsic clearance by passive diffusion through basolateral membrane of enterocytes; $R_{dif} = PS_{dif,inf}/PS_{act,inf}$; SF_{Kp}, common scaling factor for *in silico* K_p values in each tissue; T_{lag}, lag time in intestinal absorption; $V_{central}$, volume of central compartment; V_{max}, maximum uptake rate.
Values are shown as the mean ± SD.
[a]Optimized parameters of midazolam were obtained from the analyses of **Figure 4b,c**.
[b]Initial value was set as 1.
[c]Corresponding V_{max} value was calculated to be 2,086 μg/h/kg based on the following equation; $V_{max} = K_{m,u}/(1 + R_{dif}) \times CL_{int,all}/\beta$.

was estimated using the nonlinear blood concentration-time profiles after single oral doses of 150–600 mg rifampicin.[1] For the auto-induction parameters, unbound EC_{50} ($EC_{50,u}$) and E_{max} values for CYP3A induction by rifampicin were first estimated using blood midazolam concentration-time profiles after repeated oral rifampicin doses of 5–75 mg once daily.[22] The obtained $EC_{50,u}$ value for CYP3A induction was assumed to be equal to that for UGT auto-induction, based on the common involvement of pregnane X receptor-mediated induction mechanism (i.e., $EC_{50,u}$ values reflecting the binding affinity of rifampicin to the pregnane X receptor may be shared for induction of metabolic enzymes).[3] The E_{max} value for UGT auto-induction by rifampicin was estimated using its blood concentration-time profiles during 14-day repeated oral dosing of 300–900 mg rifampicin.[2] Additional rifampicin-related parameters (k_a, T_{lag}, $f_BCL_{int,all}$, and $PS_{dif,E}$) were optimized as necessary, whereas the rest of the parameters of rifampicin were set as fixed.

The estimation processes of the aforementioned $EC_{50,u}$ and E_{max} values for CYP3A induction were as follows. Midazolam parameters (k_a, T_{lag}, SF_{Kp}, f_BCL_{int}, and $V_{central}$) were first estimated using the blood midazolam concentration-time profiles after single intravenous and oral doses of midazolam only (i.e., control condition). Thereafter, the $EC_{50,u}$ and E_{max} values for CYP3A induction were estimated using the blood midazolam concentration-time profiles after rifampicin treatment (i.e., DDI condition). Specifically, the $EC_{50,u}$ and E_{max} values were determined using the DDI data of midazolam after a wide range of rifampicin doses (5–75 mg).[22] Using the obtained $EC_{50,u}$ value as fixed, the E_{max} value for UGT auto-induction was estimated. Considering that the E_{max} value for CYP3A induction might not be adequately captured with low rifampicin doses, the E_{max} value was estimated again using the different DDI data of midazolam after a high rifampicin dose (600 mg).[23] In these analyses of the DDI conditions, all of midazolam-related parameters were set as fixed with those obtained under control conditions. All of rifampicin-related parameters except for $EC_{50,u}$ and E_{max} were fixed with those obtained from auto-induction cases. For the E_{max} value for CYP2C9 induction by rifampicin, similar stepwise optimization was performed using the DDI data between rifampicin and tolbutamide.[24]

Validation of the constructed PBPK models

To validate the constructed PBPK model of rifampicin, the following simulations were performed and compared with the observed data: (i) simulations of the blood rifampicin concentration-time profiles after single oral or intravenous doses of 100–900 mg rifampicin; (ii) simulations of the CYP3A induction-mediated DDIs between rifampicin and midazolam; and (iii) simulations of the CYP3A/2C9 induction-mediated and OATP inhibition-mediated DDIs between rifampicin and glibenclamide.

RESULTS

Determination of rifampicin parameters for saturable hepatic uptake and auto-induction

Several rifampicin-related parameters were obtained by stepwise optimization (the results are summarized in **Table 1**). To adjust the distribution volume of rifampicin, the SF_{Kp} value of rifampicin was estimated using the observed blood concentration-time profiles after single intravenous doses of rifampicin (**Figure 2a**).[21] The $K_{m,u}$ value for hepatic uptake of rifampicin was determined to be 146 ng/mL using the

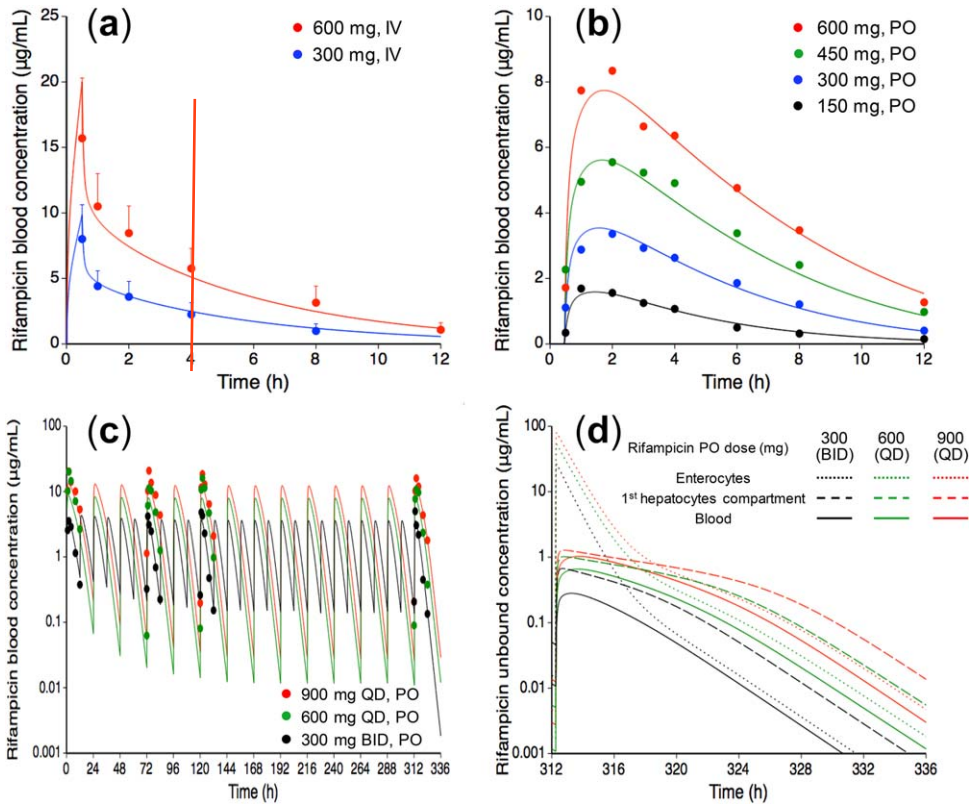

Figure 2 Optimized and observed rifampicin concentration-time profiles in blood and unbound rifampicin concentration-time profiles in blood, hepatocytes, and enterocytes after various rifampicin dosing regimens. The lines and closed circles represent optimized and observed concentration–time profiles of rifampicin, respectively. (**a**) Blood rifampicin concentration–time profiles after single intravenous infusion doses of 300 mg (blue) or 600 mg (red) rifampicin.[21] Observed data were shown as mean + SD. (**b**) Blood rifampicin concentration–time profiles after single oral doses of 150 mg (black), 300 mg (blue), 450 mg (green), or 600 mg (red) rifampicin.[1] (**c**) Blood rifampicin concentration–time profiles during 14-day repeated oral doses of rifampicin 300 mg twice daily (black), 600 mg once daily (green), or 900 mg once daily (red).[2] (**d**) Unbound rifampicin concentration–time profiles in blood (solid line), the first hepatocytes compartment (dashed line), and enterocytes (dotted line) after the last dose of 14-day repeated oral doses of rifampicin 300 mg twice daily (black), 600 mg once daily (green), or 900 mg once daily (red). The concentration–time profiles were shown with the β value of rifampicin of 0.2. Because the results shown in panels **a** and **b** were obtained in the optimization processes of PBPK model of rifampicin, auto-induction process was not incorporated.

observed nonlinear blood concentration-time profiles after single oral doses of 150–600 mg rifampicin (**Figure 2b**).[1] The parameters for saturable hepatic uptake were successfully optimized with all three β values (0.2, 0.5, and 0.8) during sensitivity analyses. However, the optimization for auto-induction cases was successful only with the β value of 0.2. The E_{max} value for UGT auto-induction by rifampicin was obtained to be 1.34 using the observed profiles with 14-day repeated oral dosing of 300, 600, or 900 mg rifampicin (**Figure 2c**).[2] In this case, the estimated trough concentrations decreased with the multiple dosing and seemed to reach a plateau on day 6. When the rifampicin concentrations at 12 hours postdosing were compared between days 6 and 1, the ratios were 0.35, 0.42, and 0.48 for rifampicin doses of 300, 600, and 900 mg, respectively. These calculated values were in good agreement with the observed values, 0.40 ± 0.20, 0.37 ± 0.12, and 0.39 ± 0.27 for the rifampicin doses of 300, 600, and 900 mg, respectively. **Figure 2d** shows the estimated unbound rifampicin concentration-time profiles in blood, hepatocytes, and enterocytes after the last dose in the auto-induction case.

To validate the obtained parameters of rifampicin related to its nonlinearity and auto-induction, the blood rifampicin concentration-time profiles after single oral or intravenous doses of 100–900 mg rifampicin were simulated. The simulated profiles were mostly in good agreement with the observed profiles (**Figure 3**[1,2,7,14,21,25–31]).

Determination of rifampicin parameters for CYP3A and CYP2C9 induction

The midazolam-related parameters were first estimated using the observed blood concentration-time profiles of midazolam under control conditions. Subsequently, the $EC_{50,u}$ and E_{max} values for CYP3A induction by rifampicin were determined to be 52.6 ng/mL and 4.29, respectively, using the observed midazolam profiles after repeated oral doses of 5–75 mg rifampicin ($EC_{50,u}$ adopted and listed in **Table 1, Figure 4a**).[22] In estimating E_{max}, the obtained $EC_{50,u}$ value (52.6 ng/mL) was

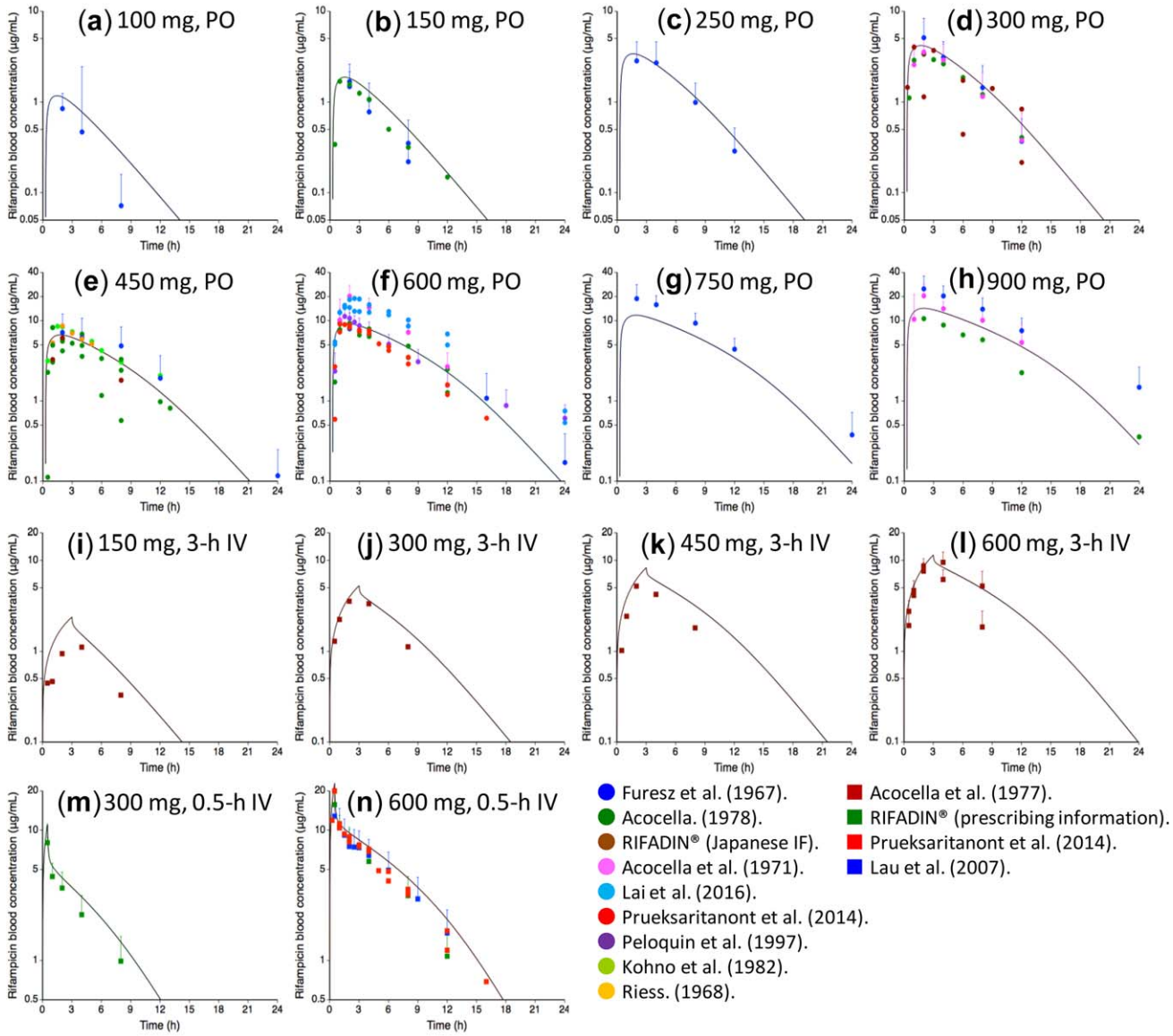

Figure 3 Simulated and observed blood rifampicin concentration-time profiles after single oral or intravenous infusion doses of 100 mg to 900 mg rifampicin. The solid lines represent simulated blood rifampicin concentration-time profiles after single oral (**a–h**) or intravenous infusion (**i–n**) doses of rifampicin. Dosing regimens are indicated in each figure. The closed circles and squares represent observed mean blood concentrations (with SD) of rifampicin after single oral or intravenous infusion doses of rifampicin, respectively. The observed data were extracted from the literature reports shown in refs. 1,2,7,14,21,25–31. IF, interview form.

used as fixed and different DDI data of midazolam after repeated oral doses of 600 mg rifampicin were analyzed.[23] The estimated E_{max} value was 4.57 (adopted and listed in **Table 1, Figure 4b-c**). During the rifampicin treatment shown in **Figure 4b,c**, time-dependent changes of the relative CYP3A activities in hepatocytes and enterocytes were shown in **Figure 4d**.

Similarly, the E_{max} value for CYP2C9 induction by rifampicin was determined to be 2.41 using the reported DDI data between rifampicin and tolbutamide (**Figure 4e**).[24] During the rifampicin treatment in **Figure 4e**, time-dependent changes of the relative CYP2C9 activities in hepatocytes were shown in **Figure 4f**.

Validation of the constructed PBPK models

Simulation of CYP3A induction effect by rifampicin

Using the obtained $EC_{50,u}$ (52.6 ng/mL) and E_{max} (4.57) values for CYP3A induction, simulations were performed to predict the CYP3A induction-mediated DDIs with midazolam. The simulated blood concentration-time profiles and AUC ratios (AUCRs) of midazolam after its single

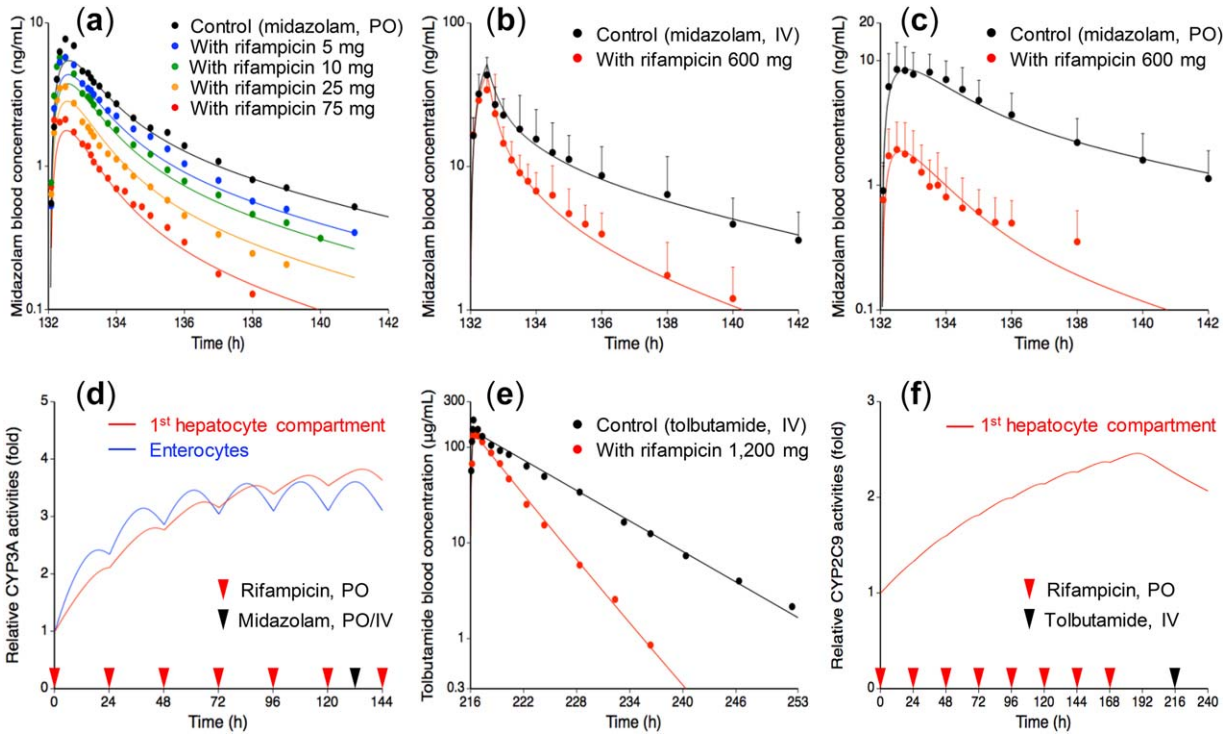

Figure 4 Optimized and observed blood concentration-time profiles of midazolam and tolbutamide before and after multiple rifampicin dosing, and the time-dependent changes in the relative cytochrome P450 (CYP)3A and CYP2C9 activities during multiple rifampicin dosing. Solid lines and closed circles represent optimized and observed data, respectively. (**a**) Blood midazolam concentration-time profiles after single oral dosing of 3 mg midazolam before (black) and after repeated oral dosing of 5 mg (blue), 10 mg (green), 25 mg (orange), or 75 mg (red) rifampicin.[22] (**b** and **c**) Blood midazolam concentration-time profiles after single intravenous infusion dosing of 0.05 mg/kg midazolam (**b**) or single oral dosing of 4 or 6 mg midazolam (**c**) before (black) and after (red) repeated oral dosing of 600 mg rifampicin.[23] Observed data were shown as mean + SD. (**d**) Estimated time courses of the relative CYP3A activities in the first hepatocyte compartment (red) and enterocytes (blue) during repeated oral dosing of 600 mg rifampicin. (**e**) Blood tolbutamide concentration-time profiles after single intravenous infusion dosing of 20 mg/kg tolbutamide before (black) and after (red) repeated oral dosing of 1,200 mg rifampicin.[24] (**f**) Estimated time course of the relative CYP2C9 activities in the first hepatocyte compartment (red) during repeated oral dosing of 1,200 mg rifampicin. The closed inverted triangles represent the timing of the doses of rifampicin (red), midazolam (black in **d**), and tolbutamide (black in **f**). Note: The results shown on the panel **a** was obtained during the optimization processes of CYP3A induction parameters by rifampicin (thus, using the unbound concentration for the half maximum induction effect ($EC_{50,u}$) and maximum induction effect (E_{max}) values of 52.6 ng/mL and 4.29, respectively).

intravenous doses after repeated oral doses of 5–75 mg rifampicin were in good agreement with the observed data (**Figure 5 and Supplementary Figure S1**).[22]

Simulation of CYP3A/2C9 induction and/or OATP inhibition effects by rifampicin

To simulate complex DDIs with glibenclamide, several glibenclamide-related parameters were first obtained by fitting to the observed profiles with glibenclamide dosing only (**Table 1 and Supplementary Figure S2**).[32] Thereafter, the complex DDIs were simulated using the parameters of rifampicin for CYP3A and CYP2C9 induction (obtained from the current study) and the previously optimized OATP inhibition parameter (unbound K_i ($K_{i,u}$) of 0.226 μmol/L).[15] For the case of oral glibenclamide dosing with single intravenous rifampicin dosing, the simulated AUCR (2.08) of glibenclamide for the β value of 0.2 was in very good agreement with the observed AUCR of 2.18 ± 1.09 (**Figure 6**).[8] In the case in which oral rifampicin dosing was repeated for 6 days followed by oral glibenclamide dosing together with single intravenous rifampicin dosing on day 7, the simulated AUCR (0.90) of glibenclamide with the β value of 0.2 was close to the observed AUCR of 0.72 ± 0.32 (**Figure 6**).[8] In the case in which repeated rifampicin dosing for 7 days followed by oral glibenclamide dosing on day 9, the simulated AUCR (0.50) of glibenclamide with the β value of 0.2 was close to the observed AUCR of 0.35 ± 0.19 (**Figure 6**).[8]

DISCUSSION

The present study aimed to construct a comprehensive PBPK model of rifampicin that can correctly and quantitatively predict complex DDIs involving the induction of CYP3A/2C9 and the inhibition of OATPs. The parameters for rifampicin and the victim drugs were individually determined using the respective blood concentration-time profiles under control conditions. Then, the rifampicin parameters for CYP3A and CYP2C9 induction were determined using the blood concentration-time profiles of midazolam and tolbutamide, respectively, after rifampicin treatment (**Figures 2–4, Table 1**). Using the obtained CYP3A induction parameters,

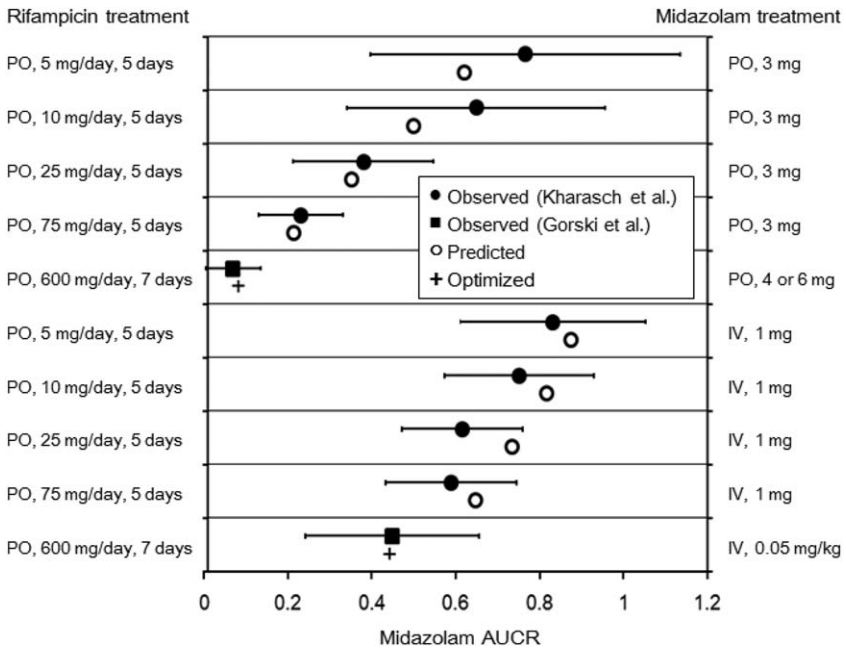

Figure 5 Optimized, simulated, and observed area under the curve ratios (AUCRs) of midazolam after repeated oral dosing of 5–600 mg rifampicin. The closed circles and squares represent observed mean AUCRs ± SD of midazolam after rifampicin treatment. The open circles and cross signs represent simulated and optimized AUCRs of midazolam after rifampicin treatment using the finally adopted estimated unbound concentration for the half maximum induction effect ($EC_{50,u}$; 52.6 ng/mL) and maximum induction effect (E_{max}; 4.57) values. Because the drug-drug interaction (DDI) data between rifampicin (PO 5, 10, 25, or 75 mg) and midazolam (PO 3 mg) were analyzed in the optimization processes with $EC_{50,u}$ (52.6 ng/mL) and E_{max} (4.29) (**Figure 4a**), the AUCRs were simulated using the finally adopted values. As the DDI data between rifampicin (PO 600 mg) and midazolam (PO 4 or 6 mg or i.v. 0.05 mg/kg) were analyzed in the final optimization process (**Figure 4b,c**), the AUCRs were calculated from **Figure 4b,c**. Because the DDI data between rifampicin (PO 5, 10, 25, or 75 mg) and midazolam (i.v. 1 mg) were used in the simulation process (**Supplementary Figure S1**), the AUCRs were calculated from **Supplementary Figure S1**. Dosing regimens of rifampicin and midazolam are indicated on both sides.

simulations for the CYP3A induction-mediated DDIs with midazolam were performed. The simulated AUCRs of midazolam were in very good agreement with the observed data (**Figure 5**). For further validation, the prediction accuracy was examined using the complex DDI cases in which intravenous and/or repeated oral doses of rifampicin were coadministered with glibenclamide. The simulated AUCRs of glibenclamide were again in quite good accordance with the observed data (**Figure 6**). Taken together, these results support the robustness and utility of our current PBPK model for rifampicin in quantitatively predicting complex DDIs with other victim drugs.

In our current study, the cases of complex DDIs between rifampicin and glibenclamide were successfully predicted for the most part. The differing impact of the glibenclamide β value on the prediction accuracy was, however, noted and it may offer an indirect clue for the rate-limiting step *in vivo*. With single intravenous rifampicin dosing (mostly incurring OATP inhibition), the simulated AUCRs of glibenclamide were independent of the β values used and very close to the observed AUCR (**Figure 6**). After multiple rifampicin dosing (mostly incurring CYP induction), the simulated AUCRs of glibenclamide varied somewhat depending on the β values used and yielded the closest prediction with the β value of 0.2 (**Figure 6**). Based on the simulation results with sensitivity analyses, the low β value of glibenclamide likely reflects *in vivo* situations in which the rate-limiting steps in the hepatic elimination of glibenclamide may be not only hepatic uptake, but also metabolism (see the Methods section). Our constructed PBPK models can adequately reflect such cases of complex DDIs.

After repeated oral dosing of rifampicin, its unbound concentrations were higher in hepatocytes than those in blood, reflecting "concentrative" hepatic uptake of rifampicin (**Figure 2d**). Moreover, the concentrative hepatic uptake was less pronounced as the unbound blood concentrations of rifampicin increased. These results support that the saturation of rifampicin hepatic uptake was adequately incorporated into the model. Of note, the optimized $K_{m,u}$ value for hepatic uptake (146 ng/mL) differed by approximately eightfold from the reported *in vitro* K_m value (1.2 μg/mL).[13] Although the exact reasons for this difference are currently unknown, albumin-facilitated hepatic uptake may contribute in part to lowering the *in vivo* K_m value. For some of the highly albumin-bound drugs, their enhanced uptake into hepatocytes by the albumin-bound form has been reported.[33] Interestingly, similar findings were also reported with K_i values for OATP inhibition by rifampicin, in that the *in vivo* K_i value was about a one-fourth of the *in vitro* K_i values.[15] For UGT auto-induction by rifampicin, the estimated $EC_{50,u}$ (52.6 ng/mL) and E_{max} (1.34) values successfully captured the auto-induction profiles, including the lowered

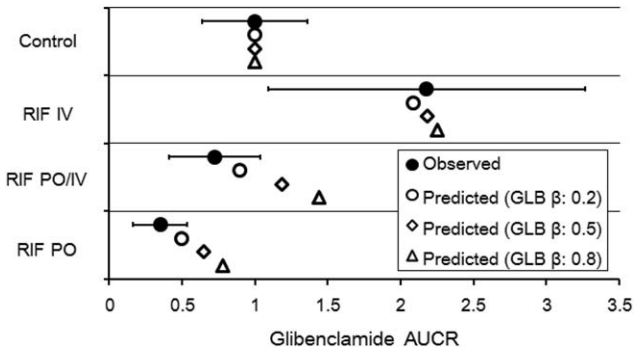

Figure 6 Simulated and observed area under the curve ratios (AUCRs) of glibenclamide with co-administration of oral and/or intravenous rifampicin (RIF) dosing. The closed circles represent observed mean AUCRs ± SD of glibenclamide with or without various co-administration of rifampicin. The open circles, diamonds, and triangles represent simulated AUCRs of glibenclamide with the β values of 0.2, 0.5, and 0.8, respectively, as a sensitivity analysis. Control: oral dosing of 1.25 mg glibenclamide (GLB) only. RIF IV: oral glibenclamide dosing with single i.v. dosing of 600 mg rifampicin. RIF PO/IV: repeated oral dosing of 600 mg rifampicin for 6 days, followed by oral glibenclamide dosing with single i.v. dosing of 600 mg rifampicin on day 7. RIF PO: repeated dosing of 600 mg rifampicin for 7 days, followed by oral glibenclamide dosing on day 9.

trough concentrations of rifampicin. However, further verification will be necessary using clinical DDI data between UGT substrates and rifampicin or other data on UGT isoforms involved in the metabolism of rifampicin.

The optimized $EC_{50,u}$ (52.6 ng/mL, 0.0639 μmol/L) and E_{max} (4.57) values for CYP3A induction by rifampicin were lower than the previously reported *in vivo* values ($EC_{50,u}$, 0.32 μmol/L; E_{max}, 15).[34] Using the obtained parameters in our current study, our PBPK model of rifampicin showed a good relationship between CYP3A induction and rifampicin doses at a wide range of 5–600 mg (**Figure 5**). However, the previously reported PBPK model did not show such relationship due to the lack of simulated DDI data with CYP3A substrates following low doses of rifampicin (<450 mg). Thus, our estimated induction parameters may be considered more reliable, but further investigations will be necessary to evaluate the prediction accuracy for CYP3A induction-mediated DDIs with other CYP3A substrates.

Overall, the obtained induction parameters for CYP3A and CYP2C9 by rifampicin yielded predictions that are in good accordance with the observed DDI data with midazolam or glibenclamide (**Figures 5 and 6**). After repeated oral dosing of 600 mg rifampicin, the estimated relative CYP3A activities were increased up to 3.8-fold and 3.6-fold in hepatocytes and enterocytes, respectively (**Figure 4d**). In the previous reports with repeated oral dosing of 600 mg rifampicin, the CYP3A protein levels in liver microsomes prepared from biopsy samples were increased by 2.4-fold to 4.7-fold.[35] Similarly, hepatic intrinsic clearance of various CYP3A substrates calculated from clinical DDI data after rifampicin treatments increased by 3.3-fold.[36] In enterocytes, the CYP3A protein levels obtained from a perfusion method or biopsy samples were increased by 3.3-fold[37] or 2.2-fold to 4.4-fold,[38] respectively, after repeated oral dosing of 600 mg rifampicin. Given that the estimated relative CYP3A activities were quite comparable to the experimentally observed values, these results support the utility of the optimized CYP3A induction parameters of rifampicin at both the liver and small intestines. Furthermore, the estimated relative CYP2C9 activities increased up to 2.5-fold in hepatocytes during rifampicin treatment (**Figure 4f**). Their increase was consistent with the increase of hepatic intrinsic clearance for various CYP2C9 substrates (by 1.3-fold to 3.7-fold) after repeated rifampicin dosing (**Supplementary Text and Supplementary Table S3**). These results also provide confidence for further use of these induction parameters in future investigations.

Regarding the major CYP isoform(s) responsible for glibenclamide metabolism, some apparent discrepancies exist. The following *in vivo* data support the major role of CYP2C9 in the hepatic metabolism of glibenclamide: (i) CYP2C9 polymorphisms significantly affected the pharmacokinetics of glibenclamide[39–42] (4.9-fold increase in its exposure in the CYP2C9 *3/*3 genotype compared to the wild type[42]); and (ii) co-administration of CYP3A inhibitors (clarithromycin, verapamil, or erythromycin) only marginally increased the glibenclamide exposure (by 1.35-fold or less[43–45]). Therefore, the estimated f_m values of glibenclamide for CYP2C9/CYP3A in the liver were 0.85/0.15, 0.94/0.06, and 1.00/0.0, respectively, when the glibenclamide β value was 0.2, 0.5, and 0.8 (see **Supplementary Text, Supplementary Table S2, and Supplementary Figure S3**). Using these f_m values and the CL_{int} ratios of each CYP2C9 genotype to the wild type,[46] the simulated AUCRs of glibenclamide for each CYP2C9 genotype to the wild type were in good accordance with the observed AUCRs (**Supplementary Figure S4**). These results further support the robustness of our constructed PBPK model of glibenclamide. Currently, information is limited on the observed AUCRs with CYP2C9 polymorphisms and the different f_m values of glibenclamide for CYP2C9 were used with varying β values. Further efforts may be needed to identify *in vivo* β value of glibenclamide. However, considering the results of DDI simulations with rifampicin, we reason that the *in vivo* β value of glibenclamide may be low. It may be worth noting that the previously reported PBPK model of glibenclamide did not succeed in predicting the AUCRs of glibenclamide for individual CYP2C9 genotypes.[47] Possible reasons for its poor prediction include: (i) the f_m value (0.35, based on the *in vitro* data) of glibenclamide for CYP2C9 was underestimated; and (ii) the β value (calculated to be >0.8) of glibenclamide was set to be high. Comparison of these different PBPK models of glibenclamide reiterates the importance of quantitative and accurate determination of the elimination mechanisms. When CYP-expressing microsomes or human liver microsomes were used, glibenclamide was reported to be metabolized primarily by CYP3A, with a minor or negligible contribution of CYP2C9.[48,49] This discrepancy in the main CYP isoforms responsible for glibenclamide metabolism between *in vivo* and *in vitro* conditions may arise from the underestimation of the CYP2C9-mediated metabolic clearance from *in vitro* experiments, in which long-chain fatty acids presented in

liver microsomes are found to suppress the activities of CYP2C9.[50]

In conclusion, the present study constructed a comprehensive PBPK model of rifampicin that can quantitatively predict complex DDIs involving CYP3A/2C9 induction and/or OATP inhibition. The constructed PBPK model adequately captured the processes of saturable hepatic uptake and auto-induction of rifampicin. The parameters of rifampicin related to CYP3A and CYP2C9 induction were obtained by stepwise optimization that used clinical DDI data with a probe substrate for CYP3A (midazolam) and CYP2C9 (tolbutamide), respectively. Using the optimized parameters, the CYP3A/2C9 induction-mediated and/or OATP inhibition-mediated DDIs with glibenclamide were successfully predicted. To our knowledge, this is the first report that successfully incorporated multiple aspects of rifampicin pharmacokinetics into a unified PBPK model. The established rifampicin PBPK model presents advancement toward accurate and quantitative prediction of DDIs with various substrates of CYP3A, CYP2C9, and/or OATPs.

Acknowledgments. The authors thank Ryo Fujino and Shinsuke Aoyama of Sekisui Medical Company, Ltd. for their experimental support of obtaining *in vitro* data of glibenclamide.

Conflict of Interest. The authors declared no conflict of interest.

Source of Funding. No funding was received for this work.

Author Contributions. R.A., K.N., H.I., W.L., and Y.S. wrote the manuscript. R.A., K.T., and Y.S. designed the research. R.A., K.T., Y.T., K.H., and Y.S. performed the research. R.A. and Y.S. analyzed the data.

1. Acocella, G. Clinical pharmacokinetics of rifampicin. *Clin. Pharmacokinet.* **3**, 108–127 (1978).
2. Acocella, G., Pagani, V., Marchetti, M., Baroni, G.C. & Nicolis, F.B. Kinetic studies on rifampicin. I. Serum concentration analysis in subjects treated with different oral doses over *a period of two weeks. Chemotherapy* **16**, 356–370 (1971).
3. Niemi, M., Backman, J.T., Fromm, M.F., Neuvonen, P.J. & Kivistö, K.T. Pharmacokinetic interactions with rifampicin: *clinical relevance. Clin. Pharmacokinet.* **42**, 819–850 (2003).
4. Maeda, K. Organic anion transporting polypeptide (OATP)1B1 and OATP1B3 as important regulators of the pharmacokinetics of substrate drugs. *Biol. Pharm. Bull.* **38**, 155–168 (2015).
5. Wienkers, L.C. & Heath, T.G. Predicting in vivo drug interactions from in vitro drug discovery data. *Nat. Rev. Drug. Discov.* **4**, 825–833 (2005).
6. Maeda, K. *et al*. Identification of the rate-determining process in the hepatic clearance of atorvastatin in a clinical cassette microdosing study. *Clin. Pharmacol. Ther.* **90**, 575–581 (2011).
7. Prueksaritanont, T. *et al*. Pitavastatin is a more sensitive and selective organic anion-transporting polypeptide 1B clinical probe than rosuvastatin. *Br. J. Clin. Pharmacol.* **78**, 587–598 (2014).
8. Zheng, H.X., Huang, Y., Frassetto, L.A. & Benet, L.Z. Elucidating rifampin's inducing and inhibiting effects on glyburide pharmacokinetics and blood glucose in healthy volunteers: unmasking the differential effects of enzyme induction and transporter inhibition for a drug and its primary metabolite. *Clin. Pharmacol. Ther.* **85**, 78–85 (2009).
9. Bidstrup, T.B., Stilling, N., Damkier, P., Scharling, B., Thomsen, M.S. & Brøsen, K. Rifampicin seems to act as both an inducer and an inhibitor of the metabolism of repaglinide. *Eur. J. Clin. Pharmacol.* **60**, 109–114 (2004).
10. Center for Drug Evaluation and Research. In Vitro Metabolism- and Transporter-Mediated Drug-Drug Interaction Studies Guidance for Industry: Draft Guidance, Food and Drug Administration, Silver Spring, MD. <https://www.fda.gov/downloads/drugs/guidancecomplianceregulatoryinformation/guidances/ucm581965.pdf> (2017). Accessed 25 October 2017.
11. Committee for Human Medicinal Products. Guideline on the Investigation of Drug Interactions, European Medicines Agency, London. <http://www.ema.europa.eu/docs/en_GB/document_library/Scientific_guideline/2012/07/WC500129606.pdf> (2012). Accessed 21 June 2012.
12. Loos, U., Musch, E., Jensen, J.C., Mikus, G., Schwabe, H.K. & Eichelbaum, M. Pharmacokinetics of oral and intravenous rifampicin during chronic administration. *Klin. Wochenschr.* **63**, 1205–1211 (1985).
13. Tirona, R.G., Leake, B.F., Wolkoff, A.W. & Kim, R.B. Human organic anion transporting polypeptide-C (SLC21A6) is a major determinant of rifampin-mediated pregnane X receptor activation. *J. Pharmacol. Exp. Ther.* **304**, 223–228 (2003).
14. Riess, W. The optimum dosage schedule for Rimactane. A Symposium on Rimactane. (Luzius Dettli, L. & CIBA Limited, Basel) 36–44 (Ciba Ltd, Basel, Switzerland, 1968).
15. Yoshikado, T. *et al*. Quantitative analyses of hepatic OATP-mediated interactions between statins and inhibitors using PBPK modeling with a parameter optimization method. *Clin. Pharmacol. Ther.* **100**, 513–523 (2016).
16. Nakagawa, H., Umene, Z. & Sunahara, S. Increased desacetylation of rifampicin and an adverse reaction. *Kekkaku.* **56**, 577–586 (1981).
17. Hisaka, A. & Sugiyama, Y. Analysis of nonlinear and nonsteady state hepatic extraction with the dispersion model using the finite difference method. *J. Pharmacokinet. Biopharm.* **26**, 495–519 (1998).
18. Chow, EC. & Pang, KS. Why we need proper PBPK models to examine intestine and liver oral drug absorption. *Curr. Drug Metab.* **14**, 57–79 (2013).
19. Yang, J., Jamei, M., Yeo, K.R., Tucker, G.T. & Rostami-Hodjegan, A. Prediction of intestinal first-pass drug metabolism. *Curr. Drug Metab.* **8**, 676–684 (2007).
20. Acocella, G., Mattiussi, R. & Segre, G. Multicompartmental analysis of serum, urine and bile concentrations of rifampicin and desacetyl-rifampicin in subjects treated for one week. *Pharmacol. Res. Commun.* **10**, 271–288 (1978).
21. Rifampin (Rifadin®) prescribing information. New Jersey (NJ): Sanofi-Aventis U.S. LLC.
22. Kharasch, E.D., Francis, A., London, A., Frey, K., Kim, T. & Blood, J. Sensitivity of intravenous and oral alfentanil and pupillary miosis as minimal and noninvasive probes for hepatic and first-pass CYP3A induction. *Clin. Pharmacol. Ther.* **90**, 100–108 (2011).
23. Gorski, J.C. *et al*. The effect of age, sex, and rifampin administration on intestinal and hepatic cytochrome P450 3A activity. *Clin. Pharmacol. Ther.* **74**, 275–287 (2003).
24. Zilly, W., Breimer, D.D. & Richter, E. Induction of drug metabolism in man after rifampicin treatment measured by increased hexobarbital and tolbutamide clearance. *Eur. J. Clin. Pharmacol.* **9**, 219–227 (1975).
25. Furesz, S., Scotti, R., Pallanza, R. & Mapelli, E. Rifampicin: a new rifamycin. 3. Absorption, distribution, and elimination in man. *Arzneimittelforschung.* **17**, 534–537 (1967).
26. Rifampin (Rifadin® capsules) Japanese interview form information. Daiichi Sankyo Co., Ltd., Tokyo.
27. Lai, Y. *et al*. Coproporphyrins in plasma and urine can be appropriate clinical biomarkers to recapitulate drug-drug interactions mediated by organic anion transporting polypeptide inhibition. *J. Pharmacol. Exp. Ther.* **358**, 397–404 (2016).
28. Peloquin, C.A., Jaresko, G.S., Yong, C.L., Keung, A.C., Bulpitt, A.E. & Jelliffe, R.W. Population pharmacokinetic modeling of isoniazid, rifampin, and pyrazinamide. *Antimicrob. Agents Chemother.* **41**, 2670–2679 (1997).
29. Kohno, H., Hata, B., Tsuchiya, T., Kubo, H. & Kobayashi, Y. Pharmacokinetics of rifampicin. *Rinshoyakuri.* **13**, 403–412 (1982).
30. Acocella, G., Bonollo, L., Mainardi, M., Margaroli, P. & Tenconi, L.T. Serum and urine concentrations of rifampicin administered by intravenous infusion in man. *Arzneimittelforschung.* **27**, 1221–1226 (1977).
31. Lau, Y.Y., Huang, Y., Frassetto, L., & Benet, L.Z. Effect of OATP1B transporter inhibition on the pharmacokinetics of atorvastatin in healthy volunteers. *Clin. Pharmacol. Ther.* **81**,194–204 (2007).
32. Neugebauer, G., Betzien, G., Hrstka, V., Kaufmann, B., von Möllendorff, E. & Abshagen, U. Absolute bioavailability and bioequivalence of glibenclamide (Semi-Euglucon N). *Int. J. Clin. Pharmacol. Ther. Toxicol.* **23**, 453–460 (1985).
33. Poulin, P. & Haddad, S. Albumin and uptake of drugs in cells: additional validation exercises of a recently published equation that quantifies the albumin-facilitated uptake mechanism(s) in physiologically based pharmacokinetic and pharmacodynamic modeling research. *J. Pharm. Sci.* **104**, 4448–4458 (2015).
34. Almond, L.M. *et al*. Prediction of drug-drug interactions arising from CYP3A induction using a physiologically based dynamic model. *Drug Metab. Dispos.* **44**, 821–832 (2016).
35. Combalbert, J. *et al*. Metabolism of cyclosporin A. IV. Purification and identification of the rifampicin-inducible human liver cytochrome P-450 (cyclosporin A oxidase) as a product of p450IIIA gene subfamily. *Drug Metab. Dispos.* **17**, 197–207 (1988).
36. Kato, M., Chiba, K., Horikawa, M. & Sugiyama Y. The quantitative prediction of in vivo enzyme-induction caused by drug exposure from in vitro information on human hepatocytes. *Drug Metab. Pharmacokinet.* **20**, 236–243 (2005).
37. Glaeser, H., Drescher, S., Eichelbaum, M. & Fromm, M.F. Influence of rifampicin on the expression and function of human intestinal cytochrome P450 enzymes. *Br. J. Clin. Pharmacol.* **59**, 199–206 (2005).

38. Greinre, B. *et al.* The role of intestinal P-glycoprotein in the interaction of digoxin and rifampin. *J. Clin. Invest.* **104**, 147–153 (1999).
39. Niemi, M., Cascorbi, I., Timm, R., Kroemer, H.K., Neuvonen, P.J. & Kivistö, K.T. Glyburide and glimepiride pharmacokinetics in subjects with different CYP2C9 genotypes. *Clin. Pharmacol. Ther.* **72**, 326–332 (2002).
40. Ieiri, I. *et al.* Pharmacogenomic/pharmacokinetic assessment of a four-probe cocktail for CYPs and OATPs following oral microdosing. *Int. J. Clin. Pharmacol. Ther.* **50**, 689–700 (2012).
41. Yin, O.Q., Tomlinson, B. & Chow, M.S. CYP2C9, but not CYP2C19, polymorphisms affect the pharmacokinetics and pharmacodynamics of glyburide in Chinese subjects. *Clin. Pharmacol. Ther.* **78**, 370–377 (2005).
42. Kirchheiner, J. *et al.* Impact of CYP2C9 amino acid polymorphisms on glyburide kinetics and on the insulin and glucose response in healthy volunteers. *Clin. Pharmacol. Ther.* **71**, 286–296 (2002).
43. Lilja, J.J., Niemi, M., Fredrikson, H. & Neuvonen, P.J. Effects of clarithromycin and grapefruit juice on the pharmacokinetics of glibenclamide. *Br. J. Clin. Pharmacol.* **63**, 732–740 (2007).
44. Semple, C.G., Omile, C., Buchanan, K.D., Beastall, G.H. & Paterson, K.R. Effect of oral verapamil on glibenclamide stimulated insulin secretion. *Br. J. Clin. Pharmacol.* **22**, 187–190 (1986).
45. Fleishaker, J.C. & Phillips, J.P. Evaluation of a potential interaction between erythromycin and glyburide in diabetic volunteers. *J. Clin. Pharmacol.* **31**, 259–262 (1991).
46. Kusama, M., Maeda, K., Chiba, K., Aoyama, A. & Sugiyama, Y. Prediction of the effects of genetic polymorphism on the pharmacokinetics of CYP2C9 substrates from in vitro data. *Pharm. Res.* **26**, 822–835 (2009).
47. Varma, M.V. *et al.* Mechanism-based pharmacokinetic modeling to evaluate transporter-enzyme interplay in drug interactions and pharmacogenetics of glyburide. *AAPS J.* **16**, 736–748 (2014).
48. Zharikova, O.L. *et al.* Identification of the major human hepatic and placental enzymes responsible for the biotransformation of glyburide. *Biochem. Pharmacol.* **78**, 1483–1490 (2009).
49. Zhou, L. *et al.* Contributions of human cytochrome P450 enzymes to glyburide metabolism. *Biopharm. Drug Dispos.* **31**, 228–242 (2010).
50. Rowland, A., Elliot, D.J., Knights, K.M., Mackenzie, P.I. & Miners, J.O. The "albumin effect" and in vitro-in vivo extrapolation: sequestration of long-chain unsaturated fatty acids enhances phenytoin hydroxylation by human liver microsomal and recombinant cytochrome P450 2C9. *Drug Metab. Dispos.* **36**, 870–877 (2008).

Supplementary information accompanies this paper on the *CPT: Pharmacometrics & Systems Pharmacology* website (http://psp-journal.com)